Towards the Effects of Initial Grain Temperature and Erosive Burning on the Solid Propellant Combustion

Doru SAFTA*,[1], Ioan ION[2]

*Corresponding author
*,[1]MTA - Military Technical Academy,
B-dul George Coşbuc 81-83, Bucharest 050141, Romania
doru.safta@yahoo.com
[2]University "Eftimie Murgu",
Piata Traian Vuia 1-4, Reşiţa 320085, Romania
ioan.resita@yahoo.com

DOI: 10.13111/2066-8201.2018.10.4.12

Received: 29 October 2018/ Accepted: 26 November 2018/ Published: December 2018

International Conference of Aerospace Sciences "AEROSPATIAL 2018"
25 - 26 October 2018, Bucharest, Romania, (held at INCAS, B-dul Iuliu Maniu 220, sector 6)
Section 6 – Experimental Investigations in Aerospace Sciences

Abstract: *On the basis of an improved mathematical model it was explored how the derived nonlinear pressure coupling response function, depending on pressure and frequency, behaves at extreme initial grain temperatures. This is accomplished by extending the existing model QSHOD (A B) to incorporate the effects of nonlinearity. Pressure - frequency analysis of nonlinear combustion response function at the pressure coupling is a relevant input of this paper and provides useful data on the occurrence of the combustion instability in the case of unsteady DB homogeneous solid propellant burning with and without erosion. A study concerning the combustion stability prediction based on the classical linear stability theory was also included in our paper. The model incorporates unsteady rotational sources and sinks in the acoustic energy assessment and thus a more accurate acoustic instability evaluation can be achieved. This method involves the computing of minimum 11 growth rate terms that arise in the dynamics of an oscillating complex flow. Finally, the paper gives an overview of some experimental results on combustion instabilities and pressure oscillations in DB solid propellant rocket motors (SPRM-01, 02 and 03). Some particular pressure-time traces, at extreme grain initial temperatures, with significant perturbed pressure signal were recorded and FFT analysed.*

Key Words: *combustion instability, Double-Base homogeneous solid propellant, unsteady burning rate, acoustic growth rate terms, pressure coupled response function*

1. COMBUSTION INSTABILITIES AND PRESSURE OSCILLATIONS IN SPRM WORKING AT EXTREME INITIAL GRAIN TEMPERATURES

1.1 Introduction

T-burner tests with temperature conditioned propellant have shown a direct link between the propellant's initial temperature and the pressure - coupled response function [11]. The prediction of combustion instability in the early design stage, considering especially the influence of the extreme initial grain temperatures, is a very difficult task due to the complex

unsteady flow field existing in the combustion chamber. The relationship between the initial grain temperature, burning rate (erosive burning) and temperature sensitivity, and their influence on the homogeneous propellant's pressure - coupled response function were explored in this paper. Our investigation of this dynamic linkage between the initial temperature and pressure - coupled response will show that of all the input parameters, the temperature-sensitivity parameter has one of the largest effects on the pressure-coupled response.

This paper is concerned with some combustion models and applications, design laboratory and full-scale tests interpretation, and prediction the behavior to be expected. The first part of the paper is focused on the assessment of the main experimental results about the combustion instabilities and pressure oscillations in the solid rocket motors (SPRM-01, 02 and 03) with DB homogeneous propellants (DBPs). Several particular pressure - time profiles at extreme ambient temperatures with significant perturbed pressure signal that was carefully FFT analysed were recorded in MTA and Electromecanica S.A. labs [2, 10].

In our paper the linearized QS theory is re-examined using a particular "*flame model*" for the condensed phase reaction zone as a high activation energy thermal decomposition model. An updated mathematical model incorporating frequency - dependent combustion response, in conjunction with pressure dependent burning, considering the erosive burning phenomenon, is applied to investigate and predict the DBP combustion instability. Several analytical predictions are presented, and some experimental validations discussed.

1.2 Rocket Motor Pressure & Thrust Measurements on the Test Stand

Our experimental researches were guided to study the DBP combustion process in 3 full scale rocket motors at extreme ambient temperatures. The motors were fired over the initial temperature range of 223 K to 323 K. Among the many experiments on the test stand (static ground tests) we recorded some particular pressure-time traces, *p(t)*, with perturbed pressure signal.

The main experiments on the test stand were done using the solid rocket motor **SPRM-01/ V01** (Fig. 2), with the following primary characteristics: $(L/D)_{SRM} = 2117/122 = 17.35$, $(L/D)_{bc}$ = 1920/114=16.84, $A_e/A_t = 3.84$ $(K_n)_i = (A_b)_i/A_t$ =335.14, 2 bates grain with inhibited ends - $(L_1)_i = (L_2)_i$ and made of a homogeneous propellant **DBP-01** (56% NC, 26.7% NG, 10.5% DNT, 3% EC, 3.8% miscellaneous; $\sigma_p = 0.00365$).

Some other investigations were done on the **SPRM-01/ V02** (Fig. 2) and **SPRM-02** built with one tubular grain made of **DBP-02/ N-4** [5]. Taking into account that downscaled motor models are relatively cheaper and their geometry that can be also modular is simpler, the experiments on the propellant **DBP-03** at extreme initial temperature were pursued using 2 smaller rocket motors, with the following characteristics: **SPRM-02**, $(L/D)_{bc} = 9.74$, $A_e/A_t = 8.5$, $(K_n)_i = (A_b)_i/A_t$ = 699.2; 1 uninhibited tubular grain - 1.140 Kg, DBP-03 and **SPRM-03**, $(L/D)_{bc} = 7.5$, $A_e/A_t = 9.0$, $(K_n)_i = (A_b)_i/A_t$ = 792.1; 1 uninhibited tubular grain - 0.850 Kg, DBP-03.

Burning rate laws, $r_{b,p}(p,T_i)$, for three DB propellants types, DBP-01, DBP-02 (similar with N-4, $\sigma_p = 0.0028$) [2, 5] and DBP-03 [10] at four different initial grain temperatures (233 K, 288 K, 300 K and 313 K), are shown in Fig. 1a and 1b. The burning rate experimental values were determined by means of the standard ballistic evaluation motor

(BEM) and of strand burner techniques, Fig. 1c. The measured pressure data (Fig. 4 – 8, 9) show a pressure spike at the beginning of the trace, which is a characteristic evidence of erosive burning. This typically occurs in motors with large aspect ratio (*L / D*) and low port area to throat area ratio or constricted flow designs such as star - aft grains. Erosive burning affects both the maximum pressure prediction early in the burn and the tail-off slope late in the burn, both of which are critical design parameters.

The advantages of accounting for the erosive burning effects in the motor design and predictions are: improved confidence in the maximum pressure prediction, improved tail-off modeling, better estimates of exposure times for insulation design, improved ignition model resolution, better estimates of pressure drop early in the burn. All of this again reduces the amount of empiricism in the ballistic model and improves predictive accuracy.

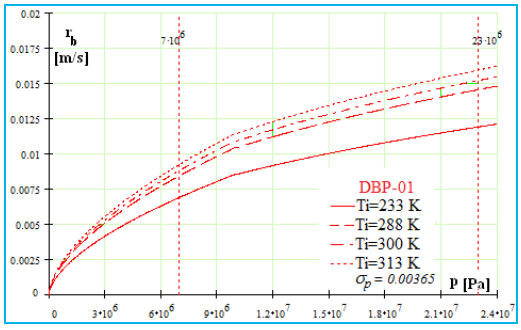

Fig. 1a - Burning rate of DBP-01

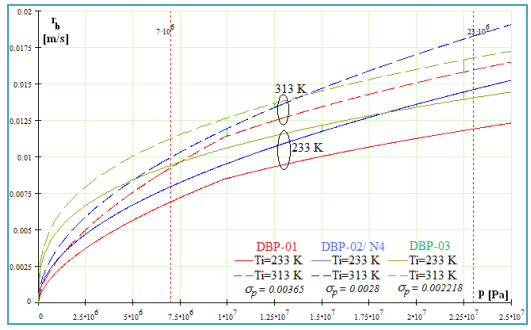

Fig. 1b - Burning rate of DBP-01, 02/ N4 and 03 at extreme initial temperatures (233 K and 313 K)

Fig. 1c - Strand Burner, Closed Bombs

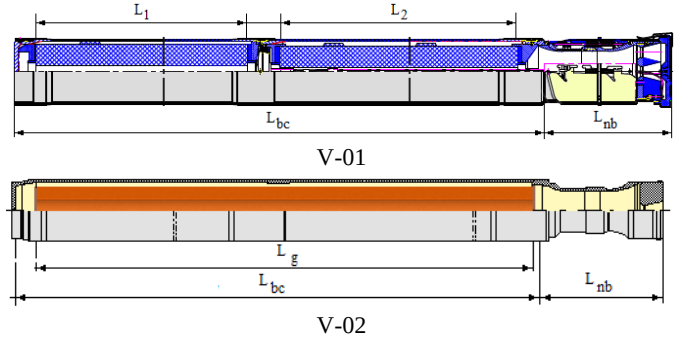

Fig. 2 - Schematic of SPRM-01 with segmented grain (V-01) and one cylindrical tube grain (V-02)

The key mechanism for erosive burning of homogeneous propellants is flame stretch, induced by an imposed velocity field [9]. This work employs one of the most widely used method, the Lenoir Robillard (L-R) model improved by R. A. Beddini, which divides the heat transfer from the flame zone back to the solid propellant into two independent mechanisms. The first, heat transfer from the primary burning zone, depends only on the pressure local value and the second one, due to combustion gases flowing over the surface, is dependent on cross flow velocity. Thus, the two burning rate terms are additive and may be defined as:

$$r_b = r_{b,p} + r_{b,e} = a_0 e^{\sigma_p (T - T_i)} p^n + \alpha \frac{G_g^{0.8}}{f(D_h)^{0.2}} e^{-\frac{\beta r_b \rho_p}{G_g}} \quad (1)$$

$$\alpha = \left(0.0288 C_{p_g} \mu_g^{0.2} \mathrm{Pr}^{-2/3}\right) \frac{1}{\rho_p C_{p_s}} \left(\frac{T_f - T_s}{T_s - T_i}\right), \tag{2}$$

$$f(D_h) = 0.90 + 0.189 D_h \left[1 + 0.043 D_h (1 + 0.023 D_h)\right], \tag{3}$$

where G_g is the gasses mass flux ($\rho_g u_g$), and $f(D_h)$ is an empirical fitted function, dependent on the hydraulic diameter D_h of the local cross section, which offers the most versatility. The hydraulic diameter is calculated using the wetted perimeter (not burning perimeter) and port area, $D_h = 4A_p / P_w$. Using (1, 2, and 3) the erosive burning contribution can be calculated using only one empirical value (β) which is essentially independent of the propellant composition and is assumed to be *53*, [13, 14]. We have also studied the influence of some other (β) values. The value of parameter α can also be assigned from empirical data rather than calculated with transport properties.

The influence of pressure and cross flow velocity of combustion gases released from burning surface on the burning rate of DBP-01 are also studied - plotted in Fig. 3. One can observe that burning rate increases almost linearly with cross flow velocity [18, 19].

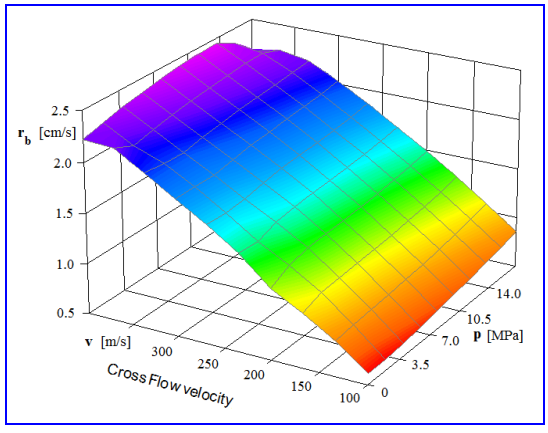

Fig. 3 - The influence of pressure and cross flow velocity on the burning rate of DBP-01.

Unstable combustion in the SPRM-01/ V-01 was often characterized by not very high pressure oscillations frequency and, sometimes, some changes of the mean burning rate occurred. Much more disturbed time - pressure profiles with linear or non-linear instabilities were recorded at very low initial temperatures corresponding of smaller pressure values (Fig. 4, 5). We can outline rather low frequency of the average pressure oscillations that have distinct amplitudes in two combustion instability zones – e.g. perturbed pressure - time history and Kernel smoothing curve at 233 K in the A detail window of Fig. 4. The most intensive perturbed and unstable combustion, with temporary pressure peaks, at the SPRM-01/ V01 occurred at the same extreme initial grain temperature of 233 K (Fig. 5 with detail window of perturbed pressure signal).

We have also noticed that combustion instabilities at higher frequencies and small amplitudes were met especially at extreme positive ambient temperatures. The pressure-time trace at 313 K presents also a rather significant variation of the average chamber pressure of

about 1 MPa in the perturbed zone (difference between the average perturbed pressure signal and non-perturbed pressure at 313 K in the A detail frame of Fig. 6). Considering the SPRM-02 with DBP-02/ N4, at 323 K, Fig. 9, one can see that after the erosive burning, the combustion instability phenomenon occurred in the second half burning time with an unstable motor working.

At sufficiently high pressure levels, corresponding to higher initial grain temperatures, all experimental static test firings were not significantly perturbed. When the pressure exceeds about 20 MPa, the oscillations of the burning rate start to grow.

For the frequency range 150–1500 Hz, common for almost of all recorded SPRM-01/ V-01 firings, the combustion instabilities were usually encountered in the axial modes.

The *p(t)* traces obtained on the test stand with SPRM-02, at 323 K, Fig. 8, 10, [10] and with SPRM-03, at 223 K, Fig. 7, [10] – static tests done by S.C. Electromecanica Ploieşti S.A., reflect quite well this phenomenon.

Thus, SPRM-02/ Ti=323 K has *p(t)* profile, Fig. 8, with one local distinct narrow perturbation zone. The perturbation region of *p(t)* extends, comprising two distinct zones, for SPRM-03 at extreme low initial temperature, Ti=223 K.

At high initial temperatures the erosive burning considerably affects the maximum pressure early in the burn (erosive over peak *>30 MPa*, e.g. Fig. 6) and also the tail-off slope late in the burn, both of them being critical design parameters.

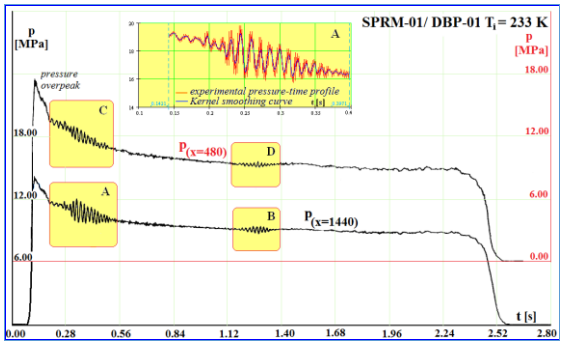

Fig. 4 - Pressure – time history, SPRM-01/ DBP-01

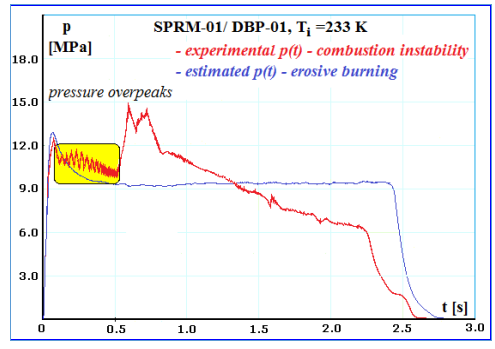

Fig. 5 - Pressure – time history, SPRM-01/ DBP-01

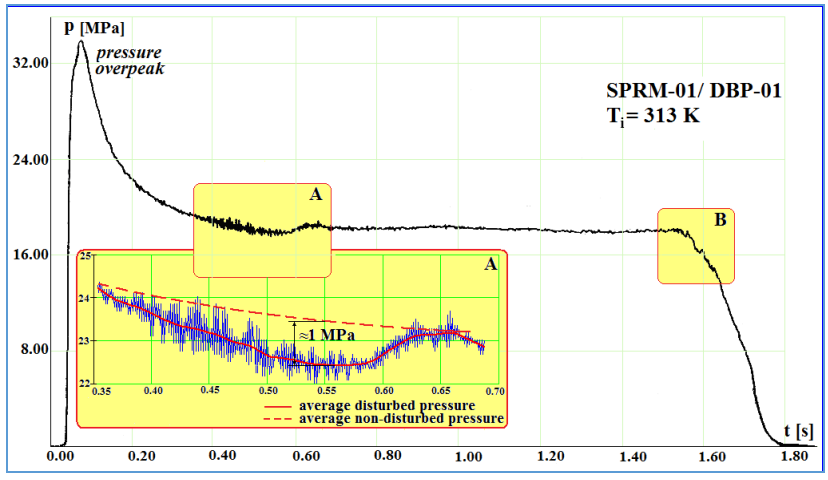

Fig. 6 - Pressure – time history, SPRM-01/ DBP-01

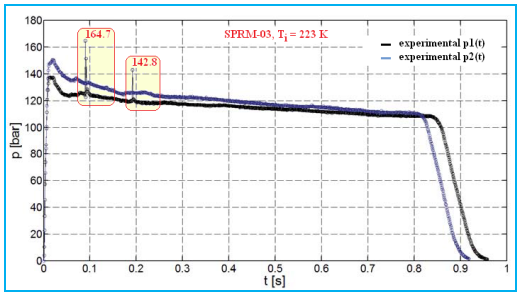

Fig. 7 - p(t) profile, SPRM-03/ DBP-03, tests of S.C. Electromecanica Ploieşti S.A. [10]

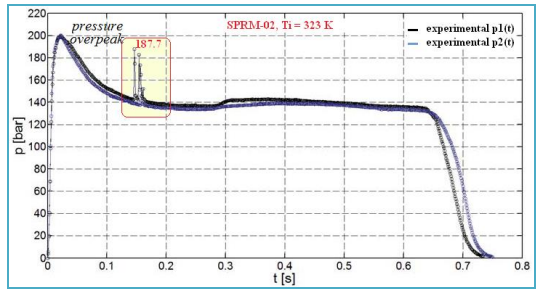

Fig. 8 - p(t) profile, SPRM-02/ DBP-03, tests of S.C. Electromecanica Ploiesti S.A. [10]

In many cases, large amplitude oscillations have been shown to develop from small disturbances in smoothly operating motors through amplification. The small disturbances usually cannot be avoided and controlling their stability becomes essential, but it is not always sufficient because large amplitude oscillations may also be triggered by initially large disturbances. Due to the unstable combustion the pressure oscillates at least 5%, usually greater 30%, and heat transfer increases, creates temporary pressure peaks and decreases the burning duration.

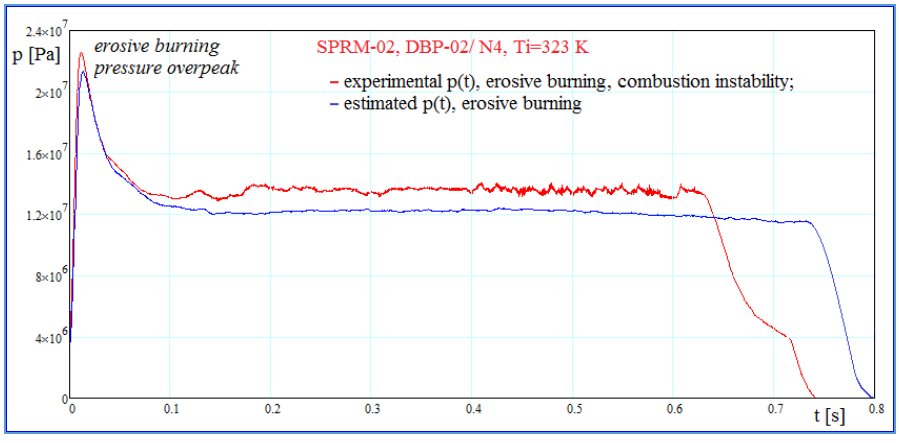

Fig. 9 - p(t) profile, at $T_i = 323\,K$, SPRM-02 with DBP-02/ N4

Fig. 10 - SPRM-03 on the test stand, S.C. Electromecanica Ploiesti S.A., [10]

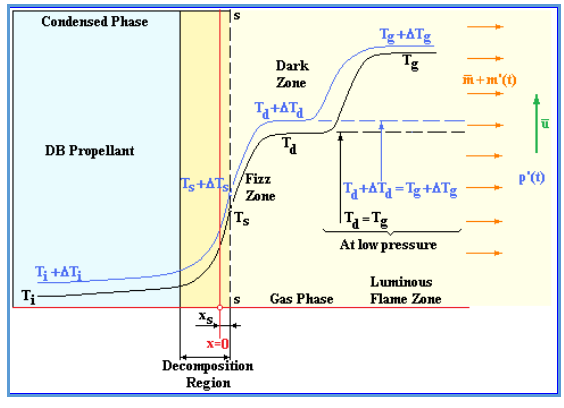

Fig. 11 - Combustion wave structure of a DBP at various initial temperatures and at high & low pressures

1.3 Analysis of the *QSHOD* Combustion Model of Homogeneous Propellants on the basis of Pressure Coupling Response Function

The present paper is concerned in a first stage with the linear stability of small pressure disturbances. The extension to the weakly nonlinear problem is approached in connection with the DBP erosive burning and SRM geometry.

In SRM the driving mechanism for combustion instability to happen is the response of the unsteady burn rate of the propellant to chamber acoustics. In our paper we will consider the *pressure coupled response*, as a response complex function for pressure fluctuations, which is the often referred parameter to describe the SRM combustion instability characteristics.

In particular, the problem is taken to be one-dimensional and all material properties are treated as quantities averaged over the chemical composition. Hence, the model is based on a non-reacting condensed phase and on a Quasi - Steady (QS) behaviour of all processes except unsteady conductive heat transfer in the condensed phase. The pyrolysis surface phenomenon is described by the Arrhenius law.

One purpose here is to take into account also the *important influence of a decomposition region within the solid phase* (Fig. 11). The conversion of condensed material to the gas phase is done at an infinitesimally thin interface and the flame is anchored on it. Sensitivity of the decomposition process can affect the combustion response in the region of maximum.

The cold un-reacted solid propellant progresses inward from the left side with a constant velocity equal with the steady state burning rate, $\bar{r}_b$ and the combustion surface oscillates around the origin during the combustion instability process, see Fig.11. The analysis of available experimental data for rocket propellants provided new arguments in the favour of the concept that the condensed phase is the locus of the burning rate control zone at the operating pressure range [1, 9].

Initial grain temperature, considered as uniform, is an external parameter without variation during operation, since only a very thin layer of the propellant is usually affected by the chemical transformation process.

Similarly with the greater part of combustion dynamics models for the pressure coupling, the linear response function R_p results in the known explicit forms (Denis and Baum, and Culick) [1-5]:

$$\left(R_p^{\ell}\right)_{DB} = \frac{m_s' / \overline{m}_s}{p' / \overline{p}} = \frac{n \cdot A \cdot B_{DB} + (\lambda - 1) n_s}{\lambda + A/\lambda - (A+1) + A \cdot B_{DB} - \dfrac{Q_r A(\lambda - 1)}{\lambda(\beta + \lambda - 1)}}, \tag{4}$$

$$\left(R_p^{\ell}\right)_{Culick} = \frac{m_s' / \overline{m}_s}{p' / \overline{p}} = \frac{n \cdot B + (\lambda - 1) n_s}{\lambda + A/\lambda - (A+1) + B - \dfrac{Q_r A(\lambda - 1)}{\lambda(\beta + \lambda - 1)}}, \tag{4'}$$

One can see that $B = B_{Culick} = A \cdot B_{DB}$. The A parameter, $A = \left(1 - T_i / \overline{T}_s\right) \cdot E$, contains the activation energy E associated with surface pyrolysis temperature T_s, and B is dependent on details of the model chosen for the processes in the gas phase, characterizing the heat feedback to the condensed phase. The A and B parameters are often practically used as floating constants to be adjusted to fit experimental data; however, they do have a theoretical basis [2, 5, and 9]. Thus, for B parameter we have chosen to use also the experimental data

obtained with T- burner technique or similar. The combustion process with decomposition zone, approached by Culick model [9], provides the pressure coupling response function in the following mathematical form:

$$R_p^{\ell} = \frac{D\left[Pn - E\left(X_p + X_{p-r}\right)\right] - EX_{-i}X_{p-i} + n_s\left[D^2 + \left(X_{-i}\right)^2\right]}{D^2 + \left(X_{-i}\right)^2},$$
$$D = X_{-r} - X_{-0} + \left(n - n_s\right)^{-1}\left[Pn - E\left(X_p + X_{P-0}\right)\right] \tag{4''}$$

The thermo-acoustic systems are generally non-normal (leading to non-orthogonality of the Eigen modes) and they may show initial transient growth for suitable initial perturbations even when the system is stable according to classical linear stability theory. The *nonlinear solid propellant response* to a pressure perturbation produced close to the combustion surface can be obtained *as an extension of the linear response derivation keeping the second order driving terms*. Even these additional terms make the models more complicated, this nonlinear model can depict some useful effects, but the linear models cannot describe them.

$$R_p^{n\ell} = R_p^{\ell} + \frac{\frac{n(n-1)}{2}B + \left(\frac{1}{2} - \frac{1}{E}\right)(\Lambda - 1)\left(R_p^{\ell}\right)^2}{\Lambda + \frac{A}{\Lambda} - (A+1) + B} \cdot \frac{p'}{\bar{p}}, \tag{5}$$

where the complex eigenvalue Λ, $\Lambda = \Lambda_r + i\Lambda_i$, must satisfy $\Lambda(\Lambda - 1) = 2i\Omega$, and Ω is defined as the dimensionless frequency, $\Omega = \lambda_p \rho_p \omega / (\bar{m}^2 c_p) = \alpha_p \omega / \bar{r}_b^2 = 2\pi\, f \alpha_p / \bar{r}_b^2$, used by Culick.

We have also derived and proposed for a weakly nonlinear case, another useful mathematical form of the response function:

$$R_p^{n\ell} = R_p^{\ell} + \left[F_1 \cdot \left(R_p^{\ell}\right)^2 + F_2 \cdot R_p^{\ell} + F_3\right] \cdot \frac{p'}{\bar{p}}, \tag{6}$$

where the coefficients are:

$$F_1 = \left[(\lambda - 1)\frac{E-2}{2E} + 1\right] \cdot \left[\lambda + A/\lambda - (A+1) + AH\right]^{-1}, \tag{7}$$

$$F_2 = \frac{n-1}{2}, \tag{8}$$

$$F_3 = \left\{\left[(\lambda - 1)\frac{2}{E} - 1\right] n_s n + (\lambda - 1)\left[-\frac{E}{E-2}\frac{n_s^2}{2} + \frac{n_s(n_s - 1)}{2} + \frac{2n_s^2}{E(E-2)}\right]\right\} \cdot \left[\lambda + A/\lambda - (A+1) + AH\right]^{-1}, \tag{9}$$

and the eigenvalue λ, as a function of Ω, must satisfy $\lambda(\lambda - 1) = i\Omega$, $\left(\lambda = \lambda_r + i\lambda_i\right)$.

We have generated several diagrams with the input data suggested by Culick [15], for the values of the pressure perturbation level 0.05 and 0.15.

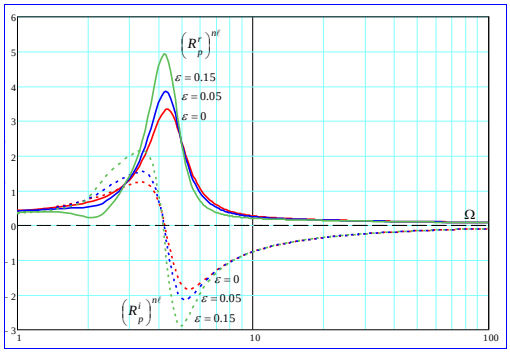

Fig. 12 - R_p^r, R_p^i,
$A = 6.0, B = 3.3, n = 0.3, \gamma = 1.18, n_s = 0$

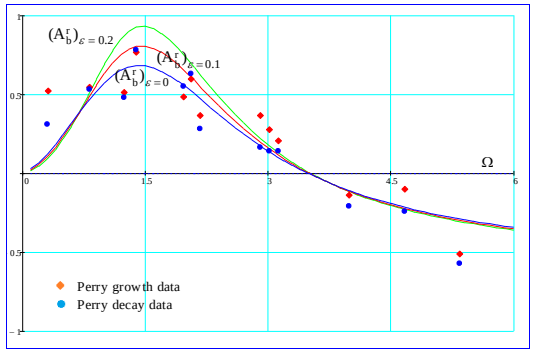

Fig. - 13 Perry's T-17 propellant data fit by the QSHOD Model: *n* = 0.82, A = 2.3, B =1.38, γ =1.18

As a good validation of the model, in the case $\varepsilon = 0$, Fig. 12 successfully reproduces the low frequency result for the response R_p^r obtained by Culick [9]. The nonlinear corrections lead to a significant increase in amplitude and a frequency shift of the primary low frequency response peak, as observed in Fig. 12.

It is important to note that this result shows that the waves receive enhanced energy flux as amplitude increases. Another reason to validate this model is the result shown in figure 13, that demonstrates a strong correlation of the admittance function to the experimental data found by Perry [16], reinforcing that the *QSHOD model does capture the low frequency behavior*.

The QSHOD theory is affected by limitations due to the assumptions made. Thus, *the main limitation refers to the failure to take into account the unsteady gas phase, which excludes the high frequency response*.

By assessing this model one can say that the lack in physical meaning of the similarity variables *A* and *B* restricts the model *to curve fitting tool for low frequency experimental data*. About these considerations, as a first step, we have analyzed the T-burner experimental data of Spurling' work [11], which performed an experimental investigation of the *relationship between temperature sensitivity and pressure-coupled response* on one particular propellant, over a broad frequency spectrum at a typical pressure (6.9 MPa). In these experiments, propellant samples along with the whole T-burner chamber, were temperature conditioned in the range of 222 K to 355 K.

The experiments revealed that *at both extreme temperatures the propellant's pressure-coupled response was significantly increased, especially at the* frequencies of around 1200 Hz and above [11]. Thus, *the largest increase of the propellant response was at higher frequencies* - the cold response seems to be worse for the first few longitudinal modes and the hot one for tangential modes and additional nonlinear behaviour. We have computed and plotted, on the basis of Eqs. (4) and (5)/ (6), the response function R_p^r, for the extreme temperatures of 222K and 355 K, at several perturbation levels, $\varepsilon = 0, 0.1 \text{and} 0.2$, taking for *A* and *B* parameters the most suitable values to fit the Spurling' T-burner data: $A = 22.933$, $B = 20.091$, $B_{DB} = 0.876$ at $T_i = 222\text{K}$; $A = 20.40$, $B = 17.60$, $B_{DB} = 0.863$ at $T_i = 355\text{K}$. It's easy to observe that the response function creates a fit to the data, Fig. 14, for low frequencies, and seems to be acceptable even for higher frequencies of 1200 Hz, up to 2500 Hz. It is important to apply an efficient method to find the most suitable values for *A* and *B* parameters.

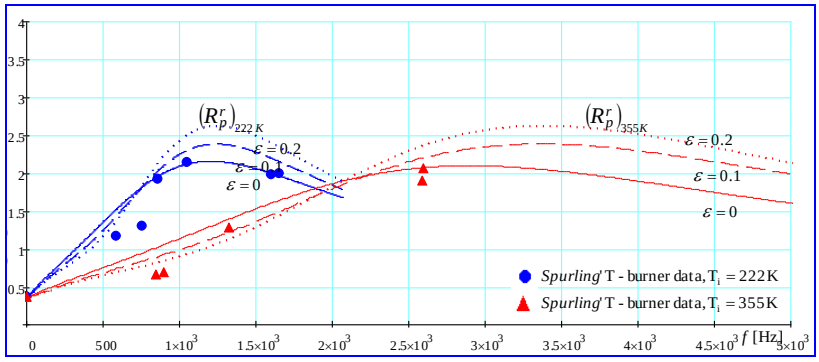

Fig. 14 - Spurling's T-burner data fit by the QSHOD Model

$$p = 6.9\,\text{MPa}\,,\ n = 0.37\,,\ \gamma = 1.16$$

Another remark concerning the practical use of QSHOD nonlinear model for DBPs is that the model is moving away from the real phenomenon when the pressure perturbation level increases $(\varepsilon > 0.1)$ in the case of small pressures $(p < p_{lim} = 2 \div 3\,MPa)$, or at extreme low initial grain temperatures.

We used the Eqs. (4) and (6) to check the response function as fitting tool for the T-burner data of Brewster work [5], *DBP-02/ N4*, at $T_i = 300\,K$, for 3 pressures, Fig. 15. Thus, the sensitive parameters have the following values: $A = 440$, $B_{DB} = 1.1$ for *p=1.5 MPa*, $A = 62$, $B_{DB} = 1.0$ for *p=5.5 MPa, and* $A = 25$, $B_{DB} = 0.95$ for *p=11 MPa*, [5].

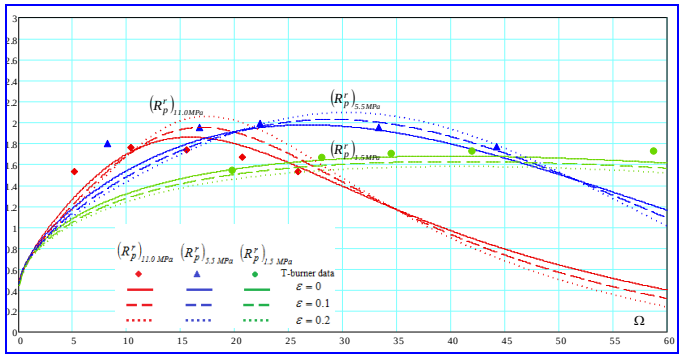

Fig. 15 - T-burner data (Brewster work [5]) fit by the QSHOD Model

DBP – 02/ N4, $p = 11.0\,MPa,\ 5.5\,MPa$ and 1.5 MPa.

Whether for the pressures of 11.0 MPa and 5.5 MPa the model works in good agreement with the experimental data, one can see that, for a pressure of 1.5 MPa, the response function magnitude decreases when the perturbation level is growing. Obviously, this issue raises a question about the applicability of the QSHOD model. In this particular case (*p=1.5 MPa* $< p_{lim}$) the abnormal evolution of the response for $\varepsilon > 0.1$, is not linked to the fitting feature of the response curves, but is certainly determined by the high frequency range when the values of *A* and *B* are not consistent with the experimental data. Another argument could be that the mentioned pressure is under the limit pressure of normal combustion of DBPs, $p_{lim} = 2.0 - 2.5 MPa$. Also, the temperature sensitivity data is highly dependent on the method of both collecting and reducing the experimental data. Although the QSHOD model is limited, *it does give insight into the solid phase contribution to the response function.*

1.4 The Influence of the Initial Grain Temperature on the Nonlinear Response of DB Propellant Combustion

On the basis of the mentioned mathematical model it was explored how the derived nonlinear pressure coupled response function behaves at extreme initial grain temperatures and when the propellant's parameters $T_s, E_s/\Re, Q_s$ and n_s take significant values in their operating ranges for DB solid propellants. This detailed parametric analysis was approached in our paper [2]. One may observe the stabilisation influence of the propellant nonlinear response for the low and high dimensionless frequency values (convergent evolution at extreme values of frequency).

This remark does not apply in the case of influence of the Arrhenius exponential law pressure exponent. The effect of the pressure perturbation level on the combustion response is considered by the factor $p'/\bar{p}$ of the nonlinear response function (Eqs. 5 and 6). Taking into account the main goal of our researches, we have investigated the behaviour of DBP-01, 02 and 03 at the extreme initial temperatures of 233 K and 313 K, for a perturbation level $p'/\bar{p} = 0.1$, (Fig. 16 and 17).

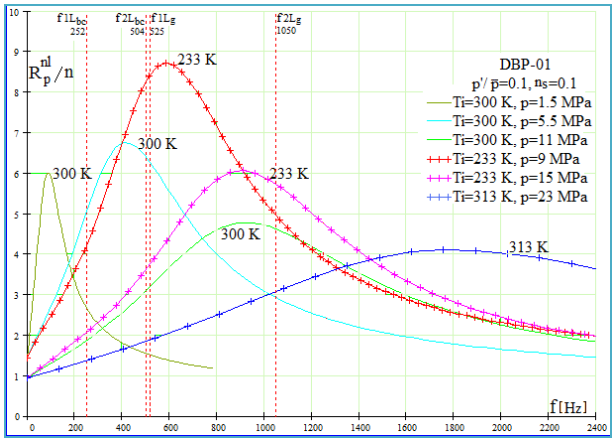

Fig. 16 - The influence of grain initial temperature on the R_p^{nl}/n ratio, DBP-01, non-erosive burning

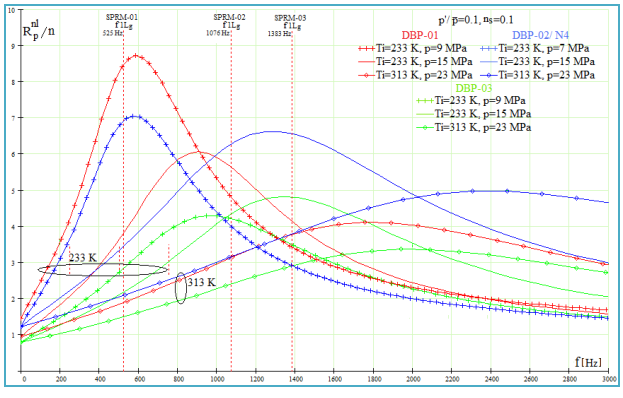

Fig. 17 - The influence of extreme initial temperatures on the R_p^{nl}/n ratio, DBP-01, 02/ N4 and 03, non-erosive burning

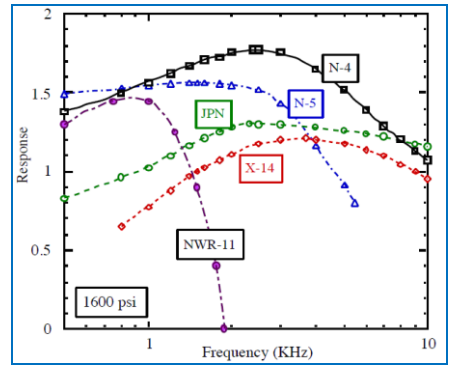

Fig. 18 - Response values of some DBPs compared to a typical AP/ HTPB prop. [17]

In this work, one can observe analysing the influence $T_i \rightarrow R_p^{nl}/n$ for DBP-01 (Fig. 16), and one of the most motor operating dangerous cases may occur at very low initial temperatures, in the range 500 – 1000 Hz.

Thus, at 233 K a higher and steep response peak occurs, depending on average chamber pressure level (7-10 MPa). The internal oscillating frequency analysis aims also to compare the fundamental acoustic longitudinal frequency, f1L, for the cylindrical grain port (SPRM-01/ V01), that is 525 Hz, with the characteristic frequency of pressure coupling response peak at 233 K - 590 Hz and 840 Hz for the mean pressures of 9 MPa and 15 MPa, Fig.16. In this frame, one can predict, for SPRM-01/ V-01, a higher risk of combustion instability phenomenon occurrence at 233 K and 9MPa, confirmed by our experimental data (Fig.4 and 5). Another remark is that a much broader and high enough response peak of the same propellant, at high conditioning temperatures (313 K) occurs when the frequency increases above 1300 Hz.

Figure 17 depicts the variation of the DBP-01, 02 and 03 nonlinear response functions, depending on frequency, at the extreme initial temperatures of 233 K and 313 K, for certain mean pressures. The fundamental acoustic longitudinal frequencies for the cylindrical grain ports of SPRM-01, 02 and 03 are mentioned on this diagram: 525 Hz, 1076 Hz and 1383 Hz. Thus, one can conclude that SPRM-01, at very low temperatures (233 K), can be much more exposed to the risk of combustion instability occurrence. However, at the same conditioning temperature, SPRM-02 and 03/ DB-03 are also susceptible to such instability but in a smaller measure thanks to the lower response amplitude in the range of 900-1400 Hz. As a good results validation the frequency values (2300 – 2500) Hz corresponding to the highest response levels of the DBP-02/ N4 obtained in this paper, see Fig. 17, are in agreement with the response values shown in Fig. 18 for N4 propellant – M. Beckstead [17].

One may also draw conclusions concerning the influences of certain propellant physical properties, such as: the characteristic frequency of the combustion dynamics increases with the propellant thermal diffusivity, relatively insensitive to mean pressure, and the sensitivity of steady-state burning to bulk temperature on the shape of response function.

2. COMBUSTION STABILITY PREDICTION BASED ON CLASSICAL LINEAR STABILITY THEORY

It is generally accepted that incorporation of unsteady rotational sources and sinks into the acoustic energy balance equation leads to a more accurate assessment of SRM acoustic instability [6, 7]. The multidimensional energy assessment involves both rotational (vortical) and irrotational (acoustic) contributions to the instantaneous pressure and velocity fields in the motor chamber. In short, they may be expanded into a series of individual integral terms that can be aggregated to obtain the total linear instability growth rate, α_T. This work involves the *calculation of minimum 11 growth rate terms* that arise in the dynamics of an oscillating complex flow. Thus, we have converted these volume stability integrals into more amenable surface forms [6, 7, 8]. The flow field properties are more accurately defined on the motor surface boundaries and allow a more precise assessment of the motor propensity for instabilities.

$$\alpha_T = \alpha_T^{irrot} + \alpha_T^{rot} = \sum_{n=1}^{4} \alpha_n + \sum_{m=5}^{11} \alpha_m = \frac{4}{5} M_b C_r \,, \tag{10}$$

where α_T^{irrot} comprises the following terms: *extended pressure coupling* (pressure coupling and nozzle damping) - $\alpha_1 = \alpha_{1c} + \alpha_{1n}$, *dilatational energy* - α_2, *acoustic mean flow* - α_3 *and particle damping* - α_4 *corrections,* and α_T^{rot} *includes: flow-turning* - α_5, *rotational flow* - α_6, *mean vortical* - α_7, *viscous* - α_8 *and pseudo acoustical* - α_9 *corrections as well as the pseudo rotational* - α_{10} *and unsteady nozzle* - α_{11} *integrals.*

Equation (10) enables a good way to find direct relations between motor parameters that will insure a stable system by guaranteeing a negative stability coefficient C_r.

In the case of neglecting the acoustic particle damping influence, for non-metalized propellants or homogeneous propellants with a very small amount of solid ingredients such as PbO, $CaCO_3$, the coefficient C_r becomes:

$$C_r = \left(A_b^r - \gamma\right) + \tfrac{1}{2} - \xi\left[\tfrac{2}{3}M_b^2 + \tfrac{1}{4}\xi^{-3}\left(1 - 2\xi + 2\xi^2 - e^{-2\xi}\right)\right] + ,$$
$$+ \tfrac{1}{2}\left(M_b^2\frac{\ell^2}{m^2}\right)\left[1 - 3M_b^2\xi^2\frac{\ell^2}{(m\pi)^2}\right] - \tfrac{4}{3}\xi M_b^2 k_m^{-1}\left(A_b^r - \gamma - 1\right) \tag{11}$$

Taking into account that condensed material in the flow has a global dynamics significant effect, the acoustic particle damping term can be evaluated by the most commonly used expression [9]:

$$\alpha_4 = \alpha_p = -\frac{C_m}{2(1+C_m)}\left[X_1\frac{1}{E_m^2}\iiint_V\left(\frac{\nabla\psi_m}{k_m}\right)^2 dV + (\bar{\gamma}-1)\frac{C}{C_p}X_2\right] = ,$$
$$-\frac{C_m}{(1+C_m)}\frac{\omega_m}{2}\left[\frac{\omega_m\tau_d}{1+(\omega_m\tau_d)^2} + (\bar{\gamma}-1)\frac{C}{C_p}\frac{\omega_m\tau_t}{1+(\omega_m\tau_t)^2}\right] \tag{12}$$

$$\tau_d = \frac{\rho_s\sigma^2}{18\mu},\ \tau_t = \left(\frac{3}{2}\frac{C_\mu}{\kappa_p}\right)\tau_d \tag{13}$$

These influence factors should be supplemented in a next study stage by corrections due to *distributed combustion* - α_{12} and *two-phase interactions* - α_{13} for a better prediction of the motor stability analysis.

Let us test the result of the linear analysis model given here by applying it to the real SPRR-01/ V01. The motor key parameters values are showed in Table 1. The distinct combustion instability cases were selected as characteristic examples for extreme initial grain temperature influence over the motor operating (Fig. 4, 5 and 6). Evaluations were done using the corrected energy normalization value, $E_m^2 = \frac{5}{8}\pi\ell$, written for axial modes in a full length cylinder.

The results of this work are evidenced in the diagram, Fig. 19, for the SRM-01/ V01 at the extreme low temperature of $T_i = 233K$.

This extended linear stability model was analysed versus three different linear stability frameworks - $(\alpha_T)_{Standard}$, $(\alpha_T)_{F2001}$ and $(\alpha_T)_{F2006}$ [7, 8, 9]. One can appreciate that α_T

calculated including 11 growth rate terms is a more comprehensive method with an estimated greater accuracy, Fig. 20.

Table 1

SRM	$\frac{\boldsymbol{L}\ [\mathrm{m}]}{\boldsymbol{R}\ [\mathrm{m}]}$	$M_b \cdot 10^{-3}$	k_m	S	$\xi \cdot 10^{-3}$
SPRM-01 $T_i = 233\,K$	$\frac{1.92}{0.057}$	11.00	*m* 0.093	8.528	1.325
SPRM-01 $T_i = 313\,K$	$\frac{1.92}{0.057}$	8.351	*m* 0.093	11.168	2.979

$$(\alpha_T)_{Standard} = \alpha_1 + \alpha_2 + \alpha_3 + \alpha_5 \tag{14}$$

$$(\alpha_T)_{F2001} = \alpha_1 + \alpha_2 + \alpha_3 + \alpha_7 + \alpha_8 \tag{15}$$

$$(\alpha_T)_{F2006} = \alpha_1 + \alpha_6 + \alpha_8 \tag{16}$$

All the results correspond to a linearly unstable system in the explored case of extreme negative initial temperatures. Hence, the stability analysis gives acceptable prediction of the observed behavior (Fig. 4, 5) - *a less stable system especially at extreme low initial grain temperatures.*

For a fixed set of physical properties, more elongated motors appear to be more susceptible to instability. The largest contributors can be readily identified to be pressure coupling, flow turning, rotational flow, mean vorticity, pseudo vorticity and unsteady nozzle corrections. The viscous term $-\alpha_8$ is $O(M_b^3)$ was ignored in Fig.19. In turbulent flow one can expect the impact of α_7 and α_8 on stability to become more significant. *The pressure of higher modes with quite appreciable amplitude accompanying the first mode data indicates nonlinear interactions that cannot be ignored.*

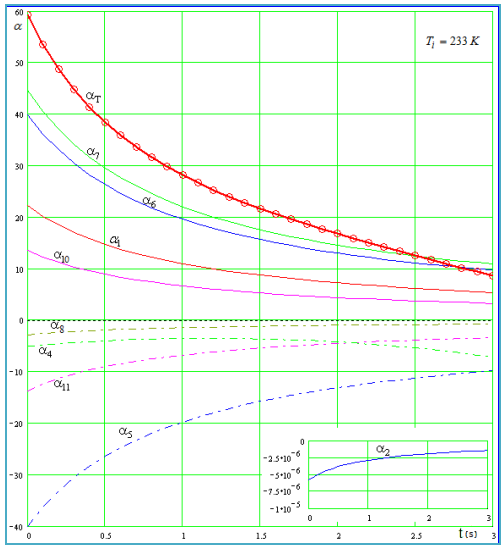

Fig. 19 - Variation in time of integral terms and total linear instability growth rate, α_T - paper model

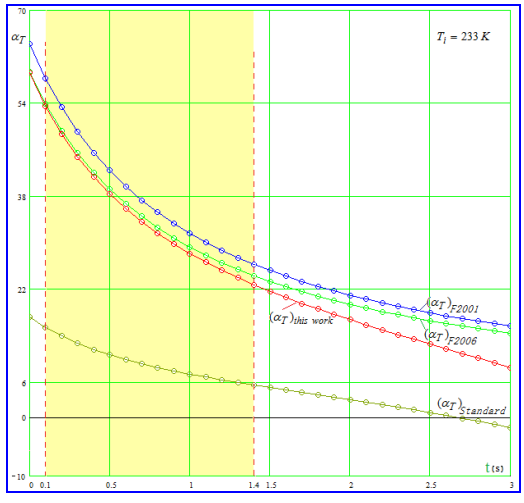

Fig. 20 - Variation in time of total linear instability growth rate, α_T , for many evaluation models

3. CONCLUSIONS

Experimental and theoretical analyses were used in tandem to offer prediction capabilities of combustion instabilities. The results of this work revealed that the *motor's size* (SPRM-01/ V01 and V02, SPRM-02 and SPRM-03) has a significant influence on transient pressure wave magnitude and structure and on the occurrence and magnitude of an associated base pressure rise.

The diagrams in Fig. 16 and 17, of the influence of grain initial temperature on the R_p^{nl}/n ratio show that one of the *most dangerous cases for the motor operating process may occur at very low initial temperatures, for frequencies up to 1000 Hz*. This remark is in agreement with the experimental researches using SPRM-01, 02 and 03 with DBP-01 and 03 at 233 K.

The mathematical form of the derived propellant response function allows taking into account the *effect of the pressure perturbation level* on the propellant unsteady combustion by the factor $p'/\bar{p}$. Very low temperatures coupled with a greater pressure perturbation level may affect the operating process by intense combustion instability (Fig. 16, 17). Our investigations on DBP-01 using SPRM-01 have enhanced that below the *threshold temperature* of ≈ 243 K the combustion instability degree may substantially increase.

Our study on the *weakly perturbed operation influence*, as well as of *erosive pressure overpeak* on the nonlinear response function have indicated their *effects of shifting of its maximum towards higher frequencies in the affected time ranges*.

Higher ratios between the free initial burning chamber volume and the nozzle critic area, coupled with low mean pressures and very low initial temperatures may offer a favourable frame for the occurrence of a violent combustion instability zone (e.g. Fig. 5, $(L^*)_{SPRM-01} = 315 > 150$). One can define a *major risk time interval* (within the burning time) correlated with the corresponding frequency variation when the risk of combustion instability occurrence becomes maxim. Thus, in the case of SPRM-01/ V01 at $T_i = 233K$ on the basis of linear instability growth rate, α_T, analysis (Fig. 19, 20) and also of the pressure - frequency diagrams of nonlinear response of DBP-01 combustion (see Fig. 16, 17) one can estimate $[0.1, 1.4]$ *sec.*, as a major risk interval. It was also learned that *higher pressure motors*, corresponding at high conditioning temperatures (313 K) and pressure oscillation frequencies above 1300 Hz, *tend to be less stable* (Fig. 16, 17).

Considerable data exist suggesting that the response function for many solid propellants tend to have higher values, in some ranges of frequencies, than predicted by the conventional QSHOD theory. Hence, the research towards predicting undesirable axial combustion instability symptoms requires a more comprehensive numerical model for internal ballistic simulation under dynamic flow and combustion conditions.

NOMENCLATURE

$A_b^{(r)} = -\boldsymbol{n}\cdot\hat{\boldsymbol{u}}/(M_b\hat{p})$ – burning surface admittance

E_s – activation energy of surface pyrolysis reaction

E – dimensionless activation energy of surface decomposition

k_m – wave number for axial mode *m*

Q_s – condensed phase heat release

$\bar{r}_b$ – steady state propellant burning rate

R_p^{ℓ}, $R_p^{n\ell}$ – propellant linear and non-linear response to the pressure coupling

δ – viscous number, $\sqrt{\nu/(a_0 R)}$

$\overline{m}$ – average mass flux

L, R – enclosure length and radius, $\ell = L / R$

m – oscillation mode shape number

M_b – surface Mach number, V_b / a_0

n – burning rate pressure exponent

λ_p , λ_g – propellant and gas phase thermal conductivity

ν, ρ – kinematic viscosity and density, μ / ρ

σ_p – sensitivity of steady-state burning to bulk temperature

ξ – viscous parameter, $m^2 \pi^2 \delta^2 l^{-2} M_b^{-3}$

n_s – pressure power in eq. of mass flux at the burning surface (Arrhenius surface pyrolysis law), $m_s = B_s p^{n_s} e^{-E_s / \Re T_s}$

REFERENCES

[1] F. S. Blomshield, *Lessons Learned In Solid Rocket Combustion Instability*, American Institute of Aeronautics and Astronautics, Missile Sciences Conference, Monterey, California, November 2006.

[2] D. Safta, T. Vasile, I. Ion, Regarding the perturbed operating process of DB propellant rocket motor at extreme initial grain temperatures, *INCAS BULLETIN*, (online) ISSN 2247–4528, (print) ISSN 2066–8201, ISSN–L 2066–8201, Vol **4**, Issue 1, DOI: 10.13111/2066-8201.2012.4.1.9, pp. 77 – 92, 2012.

[3] J. C. Traineau, M. Prevost, P. Tarrin, *Experimental low and medium frequency determination of solid propellants pressure-coupled response function, AIAA 94-3043*.

[4] N. S. Cohen, Response Function Theories That Account for Size Distribution Effects-A Review, *AIAA Journal*, Vol. **19**, No. 7, ISSN: 0001-1452, E-ISSN: 1533-385X, July 1981.

[5] M. Q. Brewster, S. F. Son, Quasi-steady Combustion Modeling of Homogeneous Solid Propellants, *Combustion and Flame* **103**: 11-26, Elsevier, ISSN: 0010-2180, 1995.

[6] S. R. Fischbach, J. Majdalani, G. A. Flandro, *Verification and validation of rocket stability integral transformations*, 41st AIAA 2005-4001/ ASME/ SAE/ ASEE Joint Propulsion Conference & Exhibit, 10-13 July 2005, Tucson.

[7] S. R. Fischbach, J. Majdalani, Volume to surface reduction of vortico-acoustic stability integrals, *Journal of Sound and Vibration* **321**, 1007-1025, 2009.

[8] S. R. Fischbach, G. A. Flandro, J. Majdalani, *Volume to surface transformations of racket stability integrals*, AIAA Paper 2004-4053.

[9] F. E. C. Culick, *Unsteady Motions in Combustion Chambers for Propulsion Systems*, RTO AGARD, AG-AVT-039, 2006.

[10] M. I. Marmureanu, thesis: *Research on the flow in the rocket engine nozzle and consequences on the dynamics of rocket flight*, "Politehnica" University of Bucharest, 2013.

[11] J. A. Spurling, F. S. Blomshield, D. Pate, *Effects of Temperature Conditioned Environment on a Propellant's Pressure – Coupled Response*, 46th AIAA 2010-7158/ ASME/ SAE/ ASEE Joint Propulsion Conference & Exhibit, 25-28 July 2010, Nashville, TN.

[12] J. A. Spurling, Effects of initial bulk temperatures on a propellant's pressure-coupled response, *International Journal of Energetic Materials and Chemical Propulsion*, Volume **12**, pp. 371-384, 2013.

[13] J. M. Lenoir, G. Robillard, *A mathematical model to predict effects of erosive burning in solid propellant rockets*, Proceeding of the 6th International Symposium on Combustion, Reinhold, New York, pp. 663-667, 1957.

[14] J. Zhang, T. L. Jackson, A model for erosive burning of homogeneous propellants, *Combustion and Flame*, in press, 2009.

[15] F. E. C. Culick, V. Yang, *Prediction of the Stability of Unsteady Motions in Solid Propellant Rocket Motors*, Nonsteady Burning and Combustion Stability of Solid Propellants, Vol. **143**, edited by L. De Luca, E. W. Price, and M. Summerfield, AIAA Progress in Astronautics and Aeronautics, Washington DC, 1992.

[16] E. H. Perry, *Investigations of the T-Burner and its Role in Combustion Instability Studies*, Ph.D. dissertation, California Institute of Technology, 1970.

[17] M. Beckstead, K. Meredith, *Examples of Unsteady Combustion in Non – Metallized Propellants*, AIAA-2000-3696, Joint Propulsion Conference & Exhibit, july 16-19, 2000, Huntsville, Alabama.

[18] I. Shih Tseng, Vigor Yang, Combustion of Double-Base Homogeneous Propellant in a Rocket Motor, *Combustion and Flame*, Volume **96**, Issue 4, March 1994, 325-342.

[19] A. Seifollahzadeh and A. Aminian, Simulation and Study of the Effect of Pressure Oscillations on Linear Combustion Instability in a Double Base Solid Rocket Motor, *J. of Chem. Eng. & Process Tech.*, 2014.